The Astrophysical Journal Letters, 979:L4 (9pp), 2025 January 20 https://doi.org/10.3847/2041-8213/ada3d8

Transonic Turbulence and Density Fluctuations in the Near-Sun Solar Wind

L.-L. Zhao[1,2], A. Silwal[2], X. Zhu[1], H. Li[3], and G. P. Zank[1,2]
[1] Center for Space Plasma and Aeronomic Research (CSPAR), The University of Alabama in Huntsville, Huntsville, AL 35805, USA; lz0009@uah.edu
[2] Department of Space Science, The University of Alabama in Huntsville, Huntsville, AL 35805, USA
[3] Los Alamos National Laboratory, Los Alamos, NM 87545, USA
Received 2024 November 27; revised 2024 December 26; accepted 2024 December 27; published 2025 January 13

Abstract

We use in situ measurements from the first 19 encounters of Parker Solar Probe and the most recent five encounters of Solar Orbiter to study the evolution of the turbulent sonic Mach number M_t (the ratio of the amplitude of velocity fluctuations to the sound speed) with radial distance and its relationship to density fluctuations. We focus on the near-Sun region with radial distances ranging from about 11 to 80 $R_\odot$. Our results show that (1) the turbulent sonic Mach number M_t gradually moves toward larger values as it approaches the Sun, until at least 11 $R_\odot$, where M_t is much larger than the previously observed value of 0.1 at and above 0.3 au; (2) transonic turbulence with $M_t \sim 1$ is observed in situ for the first time and is found mostly near the Alfvén critical surface; (3) Alfvén Mach number of the bulk flow M_A shows a strong correlation with the plasma beta, indicating that most of the observed sub-Alfvénic intervals correspond to a low-beta plasma; (4) the scaling relation between density fluctuations and M_t gradually changes from a linear scaling at larger radial distances to a quadratic scaling at smaller radial distances; and (5) transonic turbulence is more compressible than subsonic turbulence, with enhanced density fluctuations and slightly flatter spectra than subsonic turbulence. A systematic understanding of compressible turbulence near the Sun is necessary for future solar wind modeling efforts.

Unified Astronomy Thesaurus concepts: Solar wind (1534); Space plasmas (1544); Interplanetary turbulence (830)

1. Introduction

The nature of near-Sun solar wind turbulence is a foundational element of research in both solar and heliophysics, connecting coronal processes with the expanding solar wind plasma (S. R. Cranmer et al. 2017). Advected by the super-Alfvénic solar wind flow, solar wind turbulence measured near 1 au is known as weakly compressible and subsonic, with density fluctuation $\delta\rho$ typically being 10% relative to the mean density and the turbulent sonic Mach number $M_t = \delta v/c_s$ being about 0.1 (δv is the amplitude of the velocity fluctuation, and c_s is the sound speed). The compressible component of magnetic field fluctuations is also found to be only about 10% of the total magnetic fluctuation power (J. W. Belcher & J. Davis Leverett 1971). The polarization of fluctuations shows characteristics of incompressible Alfvén waves (P. J. Coleman 1968), with correlated (or anticorrelated) velocity and magnetic field fluctuations. The observed weak compressibility of solar wind has led to the wide application of incompressible turbulence theories that are usually based on low M_t values (e.g., W. H. Matthaeus et al. 1991; G. P. Zank & W. H. Matthaeus 1992, 1993). Observations of compressible turbulence are relatively rare, and therefore, compressible turbulence is poorly diagnosed. On the other hand, compressible MHD turbulence is a major topic in astrophysics, which has important implication for processes such as star formation. The pioneering work by J. Cho & A. Lazarian (2002, 2003) studied the compressible MHD turbulence with a broad range of plasma beta at different turbulent Mach numbers, including both transonic and supersonic turbulence. They decompose the MHD turbulence into Alfvén, fast, and slow modes based on the Fourier transform of velocity fluctuations. In particular, J. Cho & A. Lazarian (2002) studied supersonic sub-Alfvénic turbulence in the low-beta regime, i.e., $M_t > 1$ and turbulent Alfvén Mach number $\delta v/V_A < 1$, where V_A is the Alfvén speed. This is also the most likely condition for supersonic turbulence in the solar wind. They found that slow modes have similar spectral shape and wavevector anisotropy as the Alfvén modes, both following P. Goldreich & S. Sridhar (1995) scaling. The fast modes are isotropic with a $k^{-3/2}$ power spectrum in wavenumber k space. The density fluctuation is dominated by slow modes, and a linear scaling between density fluctuation and M_t may be expected. Other regimes such as high- and low-beta plasmas with different turbulent sonic and Alfvén Mach numbers are considered by J. Cho & A. Lazarian (2003). The spectral scaling and anisotropy of each wave mode are similar to those reported in J. Cho & A. Lazarian (2002), except that for highly supersonic ($M_t \gg 1$) low-beta plasmas, the kinetic energy spectrum of the slow modes tends to be steeper. However, solar wind turbulence near the Sun can be highly imbalanced (e.g., C. H. K. Chen et al. 2020); it remains an open question whether the previous theoretical studies on compressible balanced MHD turbulence will be applicable to this condition. Nevertheless, compressible turbulence is important and can affect the partition of heating between electrons and ions. For example, hybrid simulations by Y. Kawazura et al. (2020) in compressively driven gyrokinetic turbulence suggest that preferential electron heating requires low plasma beta and weak turbulence compressibility.

While there is a general positive correlation between turbulent sonic Mach number M_t and the relative amplitudes of density fluctuation $\delta\rho/\rho_0$ in the inertial range, there is as yet no consensus on the exact scaling relationship between the two (e.g., W. H. Matthaeus et al. 1991; L. Klein et al. 1993; G. P. Zank & W. H. Matthaeus 1993; C.-Y. Tu & E. Marsch 1994;

B. Bavassano & R. Bruno 1995; P. Hunana & G. P. Zank 2010; L. Adhikari et al. 2020). Closer to the Sun, one expects the plasma to have lower values of β (ratio between thermal pressure and magnetic pressure), which means that the sound speed c_s is smaller than the Alfvén speed V_A since $\beta \propto (c_s/V_A)^2$. Furthermore, the amplitude of the velocity fluctuations is inferred to increase with proximity to the Sun until about $10\,R_\odot$ (solar radii; S. R. Cranmer et al. 2017). One might therefore expect an increase in the M_t closer to the Sun ($\gtrsim 10\,R_\odot$) and thus, an increase in the amplitude of density fluctuation $\delta\rho/\rho_0$ (V. Krupar et al. 2020; X. Fu et al. 2022).

Besides density fluctuations, the fluctuating parallel magnetic component $\delta B_\parallel$ or the magnetic field magnitude fluctuation $\delta|B|$ is often considered to be a proxy for magnetic compressibility (C. W. Smith et al. 2006; G. G. Howes et al. 2012; C. H. K. Chen et al. 2020; L.-L. Zhao et al. 2022a), as the polarization relations of linear MHD fast and slow magnetosonic waves suggest a proportional relation between $\delta B_\parallel$ and $\delta\rho$, i.e., the positive (negative) correlation between $\delta|B|$ and $\delta\rho$ is often used to diagnose fast (slow) magnetosonic modes. However, a negative correlation between the two can also indicate nonpropagating pressure balance structures (PBSs) that may arise from the nonlinear interaction of Alfvén waves (B. J. Vasquez & J. V. Hollweg 1999). On the MHD scale, PBSs are related to slow-mode magnetosonic waves in the perpendicular limit (D. Verscharen et al. 2017). In high-speed flows, the pressure balance characteristic of the PBS may be maintained by temperature fluctuations rather than density fluctuations (G. Zank & W. Matthaeus 1990; C. Y. Tu & E. Marsch 1995; R. Bruno & V. Carbone 2013). The zero-frequency entropy mode, which contains only density fluctuations, has also been identified in the near-Sun sub-Alfvénic solar wind flow (G. P. Zank et al. 2024). In addition to the above compressible fluctuations, the spherically or arc-polarized Alfvén waves observed in the solar wind (e.g., P. Riley et al. 1996) also contain parallel magnetic fluctuations $\delta B_\parallel$ and zero-density fluctuations. However, the parametric decay of these circular-polarized Alfvén waves may lead to weak-density fluctuations (e.g., L. Del Zanna et al. 2001; M. Shi et al. 2017) as a consequence of the resonant generation of an acoustic daughter mode. The presence of nonpropagating PBSs and/or density fluctuations may reduce the Alfvénicity of the turbulence.

In this Letter, we investigate compressible fluctuations and the turbulent sonic Mach number M_t in the near-Sun solar wind using in situ observations from Parker Solar Probe (PSP) and Solar Orbiter (SolO). We examine the properties of the density fluctuations and their scaling relation to the M_t at different radial distances. The Letter is organized as follows. Section 2 focuses on the processing and selection of turbulence data from both spacecraft. Section 3 presents the results of the analysis of compressible density and magnetic fluctuations and turbulent sonic Mach number M_t. A summary and discussion are provided in Section 4.

2. Data Selection and Processing

We use publicly accessible PSP and SolO plasma and field measurements. For PSP observations, we analyze the first 19 encounter measurements from 2018 November to 2024 March. Magnetic field data are obtained from the PSP/FIELD/Fluxgate Magnetometer (MAG) instrument (S. Bale et al. 2016); electron number density n_e and core temperature T_e from PSP/FIELDS/Radio Frequency Spectrometer quasi-thermal noise (QTN) data (M. Moncuquet et al. 2020); and plasma proton velocity V_p, density n_p, and temperature T_p from Solar Probe Cup (SPC; A. W. Case et al. 2020) and SPAN-I (R. Livi et al. 2022) instruments of the PSP/SWEAP suite (J. C. Kasper et al. 2016). Plasma measurements by SPAN-I are considered only if the core of the ion velocity distribution function (VDF) falls within the field of view (FOV) of SPAN-I (P. Mostafavi et al. 2024). The PSP data set is chosen to cover a period of approximately 8 days around each perihelion, during which the plasma measurements are of relatively high cadence and the radial distances range from about 11 to 60 $R_\odot$.

SolO has completed eight orbits to date, with a minimum distance from the Sun of about 0.3 au. We use data from the five most recent orbits of SolO with a period of about 20 days centered at each perihelion, covering distances from about 60 to 80 $R_\odot$. Magnetic field data are obtained from the SolO/MAG instrument at 8 Hz (T. Horbury et al. 2020). Plasma proton moments sampled at 0.25 Hz are measured by SolO/Solar Wind Plasma Analyser (SWA)/Proton and Alpha particle Sensor (PAS; C. Owen et al. 2020). Solar wind electron density is obtained by using measurements from the SolO/Radio and Plasma Waves (RPW) instrument (M. Maksimovic et al. 2020).

The data sets are low-pass filtered using a five-point moving average before being interpolated to a uniform cadence. The individual fluctuations are first calculated by subtracting the 2 hr rolling average. Since the correlation length scale is expected to increase with radial distance (e.g., L. L. Zhao et al. 2017), we divide the data sets from the two missions into time intervals of different lengths. Specifically, the 10–60 $R_\odot$ data set from PSP measurement is split into nonoverlapping 10 minute intervals (R. Chhiber et al. 2024), while the 60–80 $R_\odot$ data set from SolO is split into nonoverlapping 30 minute intervals (L.-L. Zhao et al. 2021a). Furthermore, it is known that various solar wind turbulence features are related to the solar wind speed (S. Dasso et al. 2005; J. M. Weygand et al. 2011; L. Adhikari et al. 2021). We restrict the present analysis to the slow wind only and exclude intervals in which the bulk flow speed is greater than 450 km s^{-1}. We have also manually removed intervals associated with large-scale structures, such as heliospheric current sheet crossings (A. Szabo et al. 2020; L.-L. Zhao et al. 2021b; J. Huang et al. 2023), interplanetary shocks (L.-L. Zhao et al. 2021a; D. Trotta et al. 2024), and coronal mass ejections (T. M. Salman et al. 2024). The time-series data are then cleaned using a Hampel filter (R. Bandyopadhyay et al. 2018; M. E. Cuesta et al. 2023) within each interval. Outliers are identified as those values with an absolute difference from the interval median greater than 3 times the local standard deviation and are replaced by the local median. For PSP observations, when using SPAN-I data (e.g., SPC measurements are not available), in addition to ensuring that the ion VDF is within the FOV of the instrument, the QTN electron density n_e is preferred for calculating the Alfvén velocity and plasma beta, while the density fluctuations are calculated from the SPAN-I proton density n_p measurements due to its higher cadence and continuous data set. However, we discard intervals where the difference between $\langle n_p\rangle$ and $\langle n_e\rangle$ is larger than 0.2 times $\langle n_e\rangle$ to ensure consistency (D. Ruffolo et al. 2024). For SolO observations, if the proton density from SWA/PAS has large data gaps within the interval, the electron density estimated from the spacecraft potential measured by RPW instrument (Y. V. Khotyaintsev et al. 2021) is used.

A total of 10,779 10 minute intervals are obtained for the PSP data set, and a total of 3006 30 minute intervals remain for the SolO data set. We calculate the mean quantities and rms fluctuations within each interval. The important quantities in this study include the turbulent sonic Mach number M_t, the Alfvén Mach number M_A for the bulk solar wind flow, and the relative density fluctuation amplitude. Since the tangential velocity measurements from PSP/SPAN-I may be unreliable (R. Livi et al. 2022), only the radial bulk velocity V_R is used to calculate M_A for the entire PSP data set, i.e., $M_A = V_R/V_A$, where V_A is the Alfvén speed. The turbulent sonic Mach number is defined by the rms velocity fluctuation normalized to the sound speed $M_t = \langle \delta v^2 \rangle^{1/2}/c_s$. The sound speed c_s is calculated by $\sqrt{\gamma k_B (T_p + T_e)/m_p}$ with k_B being the Boltzmann constant. If electron temperature data are not available, we assume that proton and electron temperature are equal, and the adiabatic index $\gamma = 1.29$ (J.-B. Dakeyo et al. 2022; T. Ervin et al. 2024). The rms velocity fluctuations $\langle \delta v^2 \rangle^{1/2}$ is in principle calculated by the root of the sum of the variances of the three components, i.e., $(\langle \delta v_R^2 \rangle + \langle \delta v_T^2 \rangle + \langle \delta v_N^2 \rangle)^{1/2}$. When using PSP/SPAN-I data, it is calculated using radial and normal velocity variances, i.e., $\sqrt{\langle \delta v_R^2 \rangle + 2\langle \delta v_N^2 \rangle}$, assuming axisymmetric velocity fluctuations about the radial direction (D. Ruffolo et al. 2024). This is motivated by the distribution of the observed transverse magnetic fluctuations, i.e., $\delta b_T^2 \simeq \delta b_N^2$ from the PSP E1-E19 data set (not shown here).

3. Results: Transonic Turbulence and Density Fluctuations

Closer to the Sun, recent measurements by PSP and SolO have revealed many new findings. The first notable feature is the discovery of sub-Alfvénic solar wind, where the bulk solar wind flow velocity is less than the local Alfvén velocity, described by the Alfvén Mach number $M_A < 1$ (e.g., J. Kasper et al. 2021; R. Bandyopadhyay et al. 2022; G. Zank et al. 2022; L.-L. Zhao et al. 2022b; R. Chhiber et al. 2024). This identifies the transition from the super- to the sub-Alfvénic regime, i.e., the Alfvén critical surface. Outside the Alfvén critical surface, both inward- and outward-propagating Alfvén waves are advected outward by the solar wind. The inward-propagating Alfvén waves within the Alfvén critical surface cannot escape into the super-Alfvénic solar wind. Turbulence in the two regions may exhibit different properties (G. P. Zank et al. 2024; L. L. Zhao et al. 2022). The Alfvén Mach number M_A of the sub-Alfvén flow observed by PSP can be as low as ~0.1 (T. Ervin et al. 2024). If we suppose that the proton temperature T_p decreases with radial distance adiabatically as $r^{-4/3}$ in the near-Sun solar wind, the sound speed c_s would then exhibit a $\sim r^{-0.5}$ dependence, and this decreasing trend will be shallower due to local heating processes (L. Adhikari et al. 2024; Y. Jiao et al. 2024). According to model predictions (S. R. Cranmer et al. 2017) and PSP in situ observations (H. Wu et al. 2021), the amplitude of the velocity fluctuations δv above about 10 $R_\odot$ increases steadily as it approaches the Sun, which indicates that the turbulent sonic Mach number M_t may increase significantly closer to the Sun until about 10 $R_\odot$.

Figure 1(a) shows the probability density function (PDF) of the turbulent sonic Mach number M_t based on PSP and SolO plasma measurements. We divide the data sets from both missions into three groups based on the radial distance. The black and blue curves are from PSP observations during Encounters 1–19 with radial distance between ~10 and 60 $R_\odot$. The red curve is from SolO measurements from 2022 March to 2024 April with radial distance between ~60 and 80 $R_\odot$. Clearly, M_t moves toward larger values as one gets closer to the Sun, especially at distances between 10 and 20 $R_\odot$, with the most likely value of M_t being about 0.5. For SolO measurements beyond 0.3 au, the most probable M_t is about 0.13, which is similar to the previous studies based on Helios and 1 au observations (e.g., L. Klein et al. 1993; C. W. Smith et al. 2006). Furthermore, PSP measurements also show a distinct long tail where M_t approaches or even exceeds unity, which is known as transonic turbulence. Such turbulence has a M_t that is much larger than ~0.1 observed at and beyond 0.3 au, which could be due to a low plasma beta environment or enhanced velocity fluctuations (S. R. Cranmer et al. 2017). To our knowledge, this is the first systematic evidence that the near-Sun solar wind exhibits transonic turbulence, providing a unique opportunity to study its properties through in situ measurements. Figure 1(b) shows the radial distance dependence of the bulk flow Alfvén Mach number M_A, turbulent sonic Mach number M_t, and velocity fluctuation amplitude δV from the PSP SPAN-I data set. Each cyan scatter point is calculated at a 10 minute interval. M_A increases monotonically with radial distance r in general, as shown by the red curve in the top panel, which represents the average value of M_A in each radial distance bin. On the contrary, M_t and δV decrease with increasing radial distance beyond 10 $R_\odot$. Power-law fits are performed on the binned data, and the fitting results are listed in the figure. The M_t evolves approximately as $r^{-1.2}$. The value of M_t at the closest distance that can be measured in situ is approximately 1.

Recent observations suggest that the radial evolution of turbulence deviates significantly from the prediction of WKB theory in the sub-Alfvénic flow (L. Adhikari et al. 2022; D. Telloni et al. 2022). An important finding is that the Alfvén Mach number M_A of the solar wind flow, rather than radial distance, is the most crucial parameter for characterizing solar wind turbulence. This is because the radial profile of M_A can change significantly between different solar wind streams, which also causes a highly variable Alfvén critical surface location (R. Chhiber et al. 2024). In Figure 2(a), we show a 2D histogram of Alfvén Mach number M_A and proton beta from PSP measurements, color coded by radial distance r. The proton beta β_p positively correlates with the Alfvén Mach number M_A for the present data set. In fact, both M_A and β_p themselves vary depending on the distance from the Sun, and if this parameterization is included in the transport equation (e.g., G. P. Zank et al. 2017; A. V. Usmanov et al. 2018), one can derive their complex relationship with radial distance r. So in some sense, the turbulent properties (assuming one is in a single stream and not moving between fast and slow streams) depend only on the distance from the Sun (either a power law or a more complex relation). In the sub-Alfvénic flows, proton beta can be as low as 0.01. A power-law fit shows that M_A varies with β by about $\beta^{0.5}$. We note that, although we constrain solar wind speed to less than 450 km s^{-1} in this analysis, it is still possible that different types of streams are observed with different M_A values.

In Figure 2(b), we show the 2D histogram of M_A and M_t for the same data set as in the left panel. The color map indicates the probability density of the bin counts, where the red color represents the most likely values. The PDFs of M_A and M_t are also shown, where the most likely value of M_t is about 0.5,

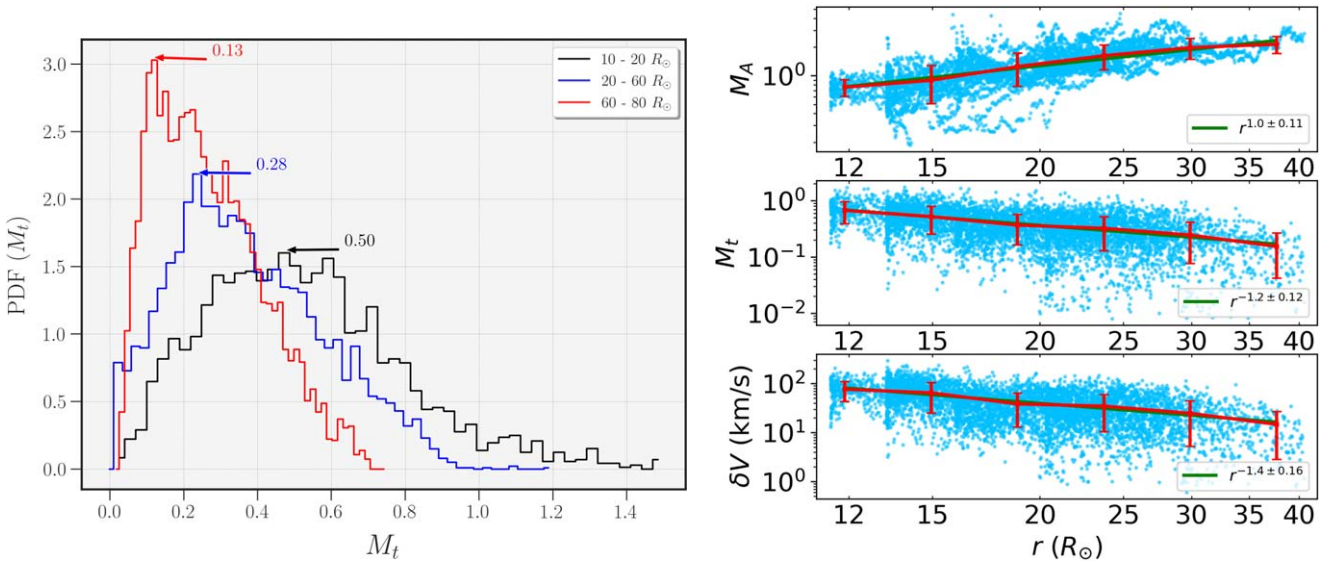

Figure 1. The left panel shows the normalized histograms that represent the probability density function (PDF) of the turbulent sonic Mach number M_t for three heliocentric distance ranges observed by PSP and SolO. The histogram is normalized so that the area under each curve is equal to 1. The right panel shows the radial distance dependence of the bulk flow Alfvén Mach number M_A, turbulent sonic Mach number M_t, and the amplitude of velocity fluctuation δV calculated at 10 minute intervals from the PSP data set.

while M_A has two most probable values in our data set, which may be due to the different solar wind streams associated with different values of M_A as discussed earlier. It is clear that when M_A becomes close to or less than 1, M_t shifts to larger values and even exceeds 1. As shown in Figure 1, M_t observed by SolO at about 0.3 au and above is likely about 0.1. However, as PSP gets closer to the Sun, in addition to the observation of sub-Alfvénic flow, another notable feature is the appearance of transonic turbulence, i.e., M_t steadily increases, far exceeding 0.1. This is also reflected in Figure 2(b), where most of the M_t values in the sub-Alfvén region (the region below the horizontal dashed line) are greater than 0.1. From Figure 2(b), it is also interesting to note that the trend of increasing M_t with decreasing M_A somewhat halts near the Alfvén critical surface. This can be seen from the histogram of the intervals with $M_t > 1$ (i.e., the region to the right of the vertical dashed line in Figure 2(b)), where the larger PDFs are observed near the $M_A \sim 1$ horizontal dashed line. The large M_t values observed near the Alfvén surface may be due to the stagnation of the inward-propagating Alfvén waves and the subsequent nonlinear interaction with the outward Alfvén modes (e.g., A. Verdini & M. Velli 2007) or the possible parametric decay process in the low-beta ($\beta \ll 1$) regime generating compressive acoustic modes (e.g., F. Malara & M. Velli 1996).

The turbulent sonic Mach number M_t is closely related to compressible density fluctuations, and the high value of M_t observed close to the Sun as shown in Figures 1 and 2 could greatly affect the solar wind density fluctuations (e.g., V. Krupar et al. 2020; X. Fu et al. 2022). Previous studies based on low M_t observations have provided a correlation between density fluctuation $\delta\rho/\rho_0$ and M_t in the inertial range (e.g., W. H. Matthaeus et al. 1991; L. Klein et al. 1993; B. Bavassano & R. Bruno 1995; G. Zank et al. 1990) though a consensus is still elusive. Recent compressible local box MHD simulations have found a linear scaling between the two (X. Fu et al. 2022; S. Du et al. 2023), consistent with observations from the first eight encounters of PSP (M. E. Cuesta et al. 2023). Here, we examine the scaling relation between density fluctuations and M_t in the near-Sun solar wind using unprecedented in situ measurements from the first 19 orbits of PSP and most recent data from SolO. The radial distance can be as close as about 10 $R_\odot$. Figure 3 shows the evolution of the relative proton density fluctuations and its dependence of M_t with radial distance from about 10 to 80 $R_\odot$. We divide the data sets from the two missions into four subsets based on the radial distance r range, which is shown on a logarithmic scale on the horizontal axis. Panels from left to right represent the scaling relation of density fluctuations in (a) 10–20 $R_\odot$, (b) 20–40 $R_\odot$, (c) 40–60 $R_\odot$, and (d) 60–80 $R_\odot$. The flow speed in the entire data set is less than 450 km s^{-1}. Similar to Figure 2(a), we plot the 2D histogram of M_t versus $\langle \delta n_p^2 \rangle^{1/2} / \langle \delta n_p \rangle$ (henceforth $\delta\rho/\rho_0$) in each panel, color coded by the sampling angle $\theta_{V\,B}$. The power-law fit between M_t and $\delta\rho/\rho_0$ is shown as the black line, and the fitted power-law exponent is also given. The red arrows in each panel indicate the average values of M_t and $\delta\rho/\rho_0$ in each distance range, which can be different from the most likely values. The red asterisk is the combination of the two averages. The sampling angle $\theta_{V\,B}$ mostly is quasi-parallel for the present analysis but does have an obvious dependence on radial distance. Quasi-perpendicular sampling is shown only at larger radial distances observed by SolO. Previous studies have shown that the power anisotropy of density fluctuations is angle dependent, with larger sampling angles generally being associated with larger density fluctuations (S. Du et al. 2023; J. Wang et al. 2024). Despite the relatively narrow range of sampling angles at such close distances, our results show similar trends within each radial distance bin, i.e., larger $\theta_{V\,B}$ is accompanied by larger $\delta\rho/\rho_0$. It is also clear that the average values of M_t increase slightly with decreasing distance as indicated by the shift of red arrows. The amplitude of the density fluctuations does not vary much but increases slightly at 10–20 $R_\odot$. In addition to the above features, another prominent feature is a systematic change of the $\delta\rho/\rho_0$ versus M_t scaling relation with radial distance. The scaling appears to change from approximately

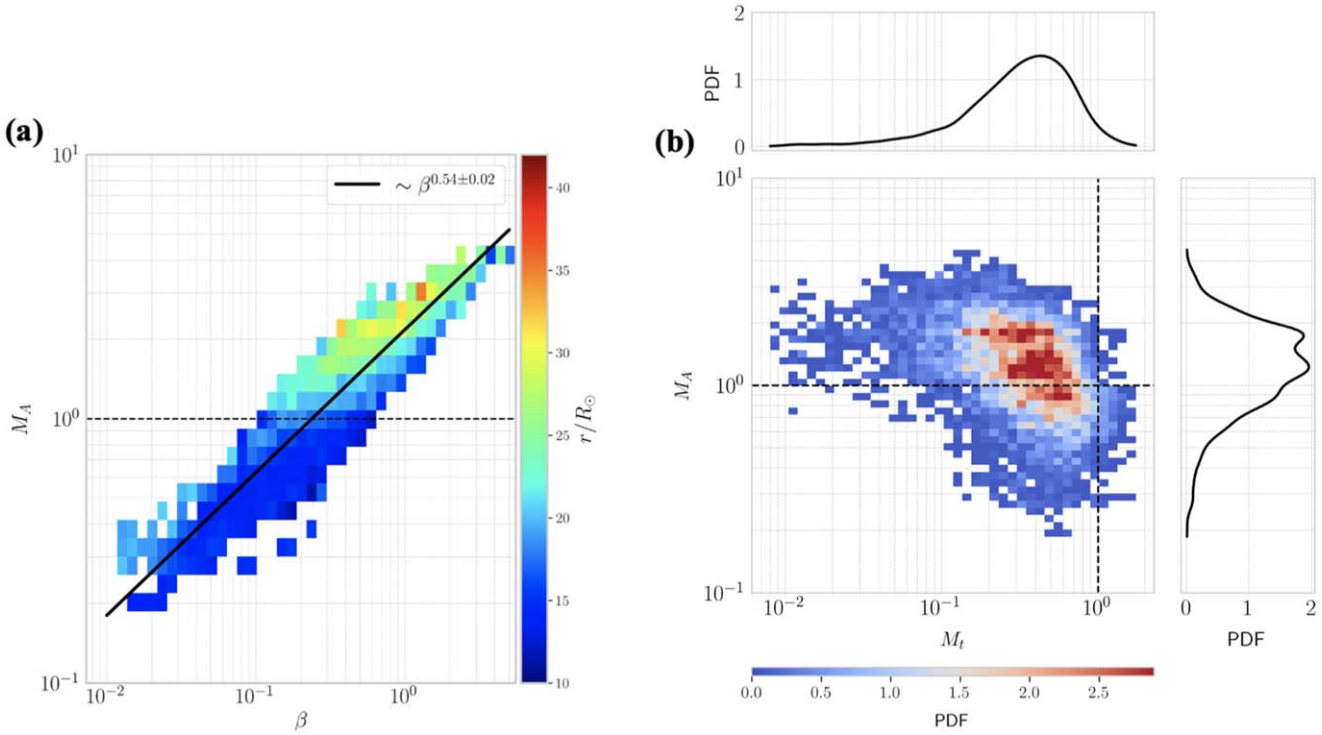

Figure 2. The left panel shows a 2D histogram of Alfvén Mach number M_A and proton beta β from PSP measurements. The right panel shows a 2D histogram of M_A and M_t, with the color map indicating the PDF of bin counts. The PDFs of M_A and M_t are shown on the top and right, respectively.

quadratic at a distance close to the Sun to linear scaling farther away. The reason may be due to the change in plasma conditions (e.g., β and cross helicity) or in the nature of compressive fluctuations. The traditional nearly incompressible (NI) theory of turbulence in a homogeneous flow suggests $\delta\rho/\rho_0 \propto M_t^2$ (G. P. Zank & W. H. Matthaeus 1992, 1993), with density fluctuations being generated by a pseudosound process, in which the density variations follow the eigenrelation of sound waves but are produced by incompressible fluid motions. With spatial inhomogeneities in an expending solar wind, a linear scaling $\delta\rho/\rho_0 \propto M_t$ can be expected (A. Bhattacharjee et al. 1998; P. Hunana & G. P. Zank 2010; L. Adhikari et al. 2020). At distances close to the Sun, the young solar wind is less developed with high Alfvénicity and cross helicity. With increasing distance, the plasma gradually evolves to a fully developed turbulent state (C. H. K. Chen et al. 2020; D. Telloni et al. 2021). This shift in the scaling relation of density fluctuations appears to be explainable by the NI theory, with the inhomogeneities increasing as the solar wind expands outward. However, it cannot be ruled out that the driving force for compressible fluctuations in the low-β and highly imbalanced solar wind regime has changed. For example, the possible excitation of the parametric decay instability (PDI) of Alfvén waves close to the Sun may affect the properties of density fluctuations and their scaling with M_t (e.g., T. A. Bowen et al. 2018; X. Fu et al. 2022; G. Zank et al. 2022; C. González et al. 2023). To determine the exact reasons for this shift in density fluctuation scaling, simulations are still needed with similar near-Sun plasma conditions to explore quantitatively.

Previous studies often use the correlation between the fluctuations in the magnetic field strength $|B|$ and proton density n_p to roughly examine the nature of compressive fluctuations observed in the solar wind (G. G. Howes et al. 2012; S. Bale et al. 2019; C. H. K. Chen et al. 2020). A general anticorrelation between the two is often reported in the distant solar wind (e.g., G. G. Howes et al. 2012). This is revisited with the present PSP data set near the Sun. The magnetic field data are downsampled to the same time resolution as the plasma measurements within each interval. We describe the correlation using the standard Pearson correlation coefficient. The left panel of Figure 4 shows the 2D histogram of the correlation coefficient $C(\frac{\delta n_p}{n_p}, \frac{\delta|B|}{|B|})$ and proton beta using PSP E1-E19 data at distances of $\sim$10–60 $R_\odot$. Obviously, although the fluctuations between $|B|$ and n_p in some regions show a positive correlation, the probability of a negative correlation between the two is relatively large. The proton β values are mainly between 0.1 and 1, and the dependence of the correlation coefficient on β is not very clear, probably due to the limited data set. The most probable interpretation of a negative correlation probably indicates the presence of slow-mode waves. However, the negative correlation between the two is much weaker than the observation at 1 au, which is close to -1. This suggests that the relative contributions of various compressive wave modes near the Sun may have changed (G. P. Zank et al. 2024). For example, the possible presence of zero-frequency entropy mode, which contains only density fluctuations, could reduce this anticorrelation. Furthermore, nonpropagating PBSs, which are usually interpreted as the perpendicular propagating slow modes, may also reduce this anticorrelation as the pressure balance characteristics in the PBSs can be maintained by temperature fluctuations (e.g., G. Zank et al. 1990; C. Y. Tu & E. Marsch 1995). The right panel of Figure 4 shows the probability distribution of the proton density fluctuations using the present PSP and SolO data sets. We divide the data set into three subsets based on the same radial distance range as in the left panel of Figure 1. The most likely value of the normalized density fluctuations in all three regions is around 0.1. However, it is clear that the peak

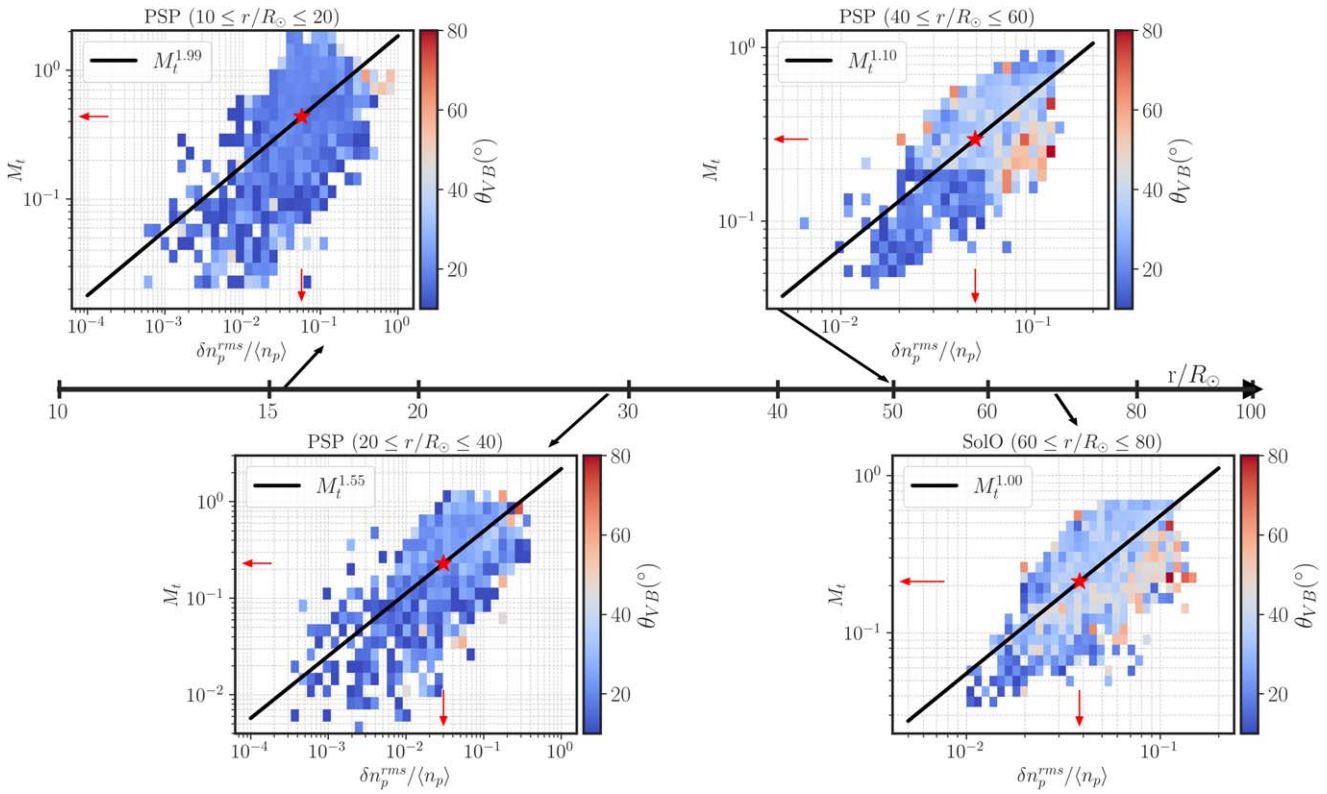

Figure 3. Radial evolution of the scaling relation between the density fluctuation $\delta\rho/\rho_0$ and M_t observed by PSP and SolO from 10 to 80 $R_\odot$. The panels from left to right show the scaling of density fluctuations in radial distances of 10–20 $R_\odot$, 20–40 $R_\odot$, 40–60 $R_\odot$, and 60–80 $R_\odot$, respectively. Each panel represents a 2D histogram of $\delta\rho/\rho_0$ vs. M_t, color coded by the sampling angle θ_{VB}. The red asterisk in each panel indicates the average values of M_t and $\delta\rho/\rho_0$ in each distance range.

value of $\delta n_p/n_p$ shifts to larger values when the distance gets closer to the Sun. In addition, through nonlinear least-squares fitting, the density fluctuation distributions in the three regions all conform to the lognormal distribution, as shown by the solid curves. The fitting results show that the standard deviation is small (less than 0.1 in all three regions). The lognormal distribution of the plasma density has been reported before (e.g., L. Burlaga & A. Szabo 1999), and we show here that density fluctuations also have this distribution, which is a natural consequence of a large number of random, uncorrelated multiplicative perturbations that converge to a lognormal distribution via the central limit theorem. There are high-density fluctuations in the tail that deviate slightly from the lognormal distribution, which may be related to the relatively high turbulent Mach number there.

We further use PSP observations to investigate the fluctuation spectral properties with increasing M_t. Figure 5 shows an example of the comparison of the magnetic fluctuation trace spectra (left panel) and the proton density spectra (right panel) for different ranges of M_t values in the PSP Encounter 19 observations. We resample the 10 minute PSP data set to 1 hr and divide the data set into five groups according to the range of M_t values. The power spectra are calculated at 1 hr intervals and then averaged in each M_t group. To untangle the effects of M_t, we constrain all possible independent solar wind parameters to be similar. The 5th-to-95th-percentile range of each solar wind parameter in Figure 5 is about 0.1–0.4 for proton beta β, 12–30 $R_\odot$ for radial distance r, 5°–30° for the sampling angle θ_{VB}, and 0.5–0.9 for the normalized cross helicity σ_c. As shown in the figure, in the frequency range above ∼0.005 Hz, the amplitudes of both incompressible magnetic trace spectra and compressible density spectra increase with the increasing M_t, which may due to the fact that the larger M_t turbulent flows are primarily caused by the enhanced velocity fluctuations. However, the opposite is observed in the low-frequency density fluctuation spectra, i.e., small M_t group has a larger fluctuation amplitude, which is clearer when we use Fourier transform to perform spectral analysis (not shown here). This leads to a shallower (or flatter) density spectrum when M_t is larger. The black dashed lines indicate the power-law fits in the frequency range from 10^{-2} to 10^{-1} Hz. The spectral index of the density fluctuation changes from about −1.87 to −1.4 as M_t increases from 0.1 to 1. Although a very slight flattening is also observed in the magnetic fluctuation trace spectra when M_t is large, the overall spectral index does not seem to be much affected by M_t compared to the density fluctuations, probably because M_t is mainly related to the compressibility fluctuations.

4. Discussions and Conclusions

In this work, we analyzed aspects of the turbulent sonic Mach number M_t and MHD-scale compressible fluctuations by recent PSP and SolO measurements. The radial distances cover the closest region accessible by in situ solar wind observations, ranging from ∼10 to 80 $R_\odot$, with a focus on the transition near the Alfvén critical surface. The bulk flow speed is limited to less than 450 km s^{-1}, appropriate to slow solar wind study. Our analysis revealed the following key observational properties.

1. On average, the turbulent sonic Mach number M_t (i.e., the ratio of the amplitude of velocity fluctuations to the speed of sound) moves steadily toward larger values with decreasing radial distance from the Sun and persists until at least 11 $R_\odot$,

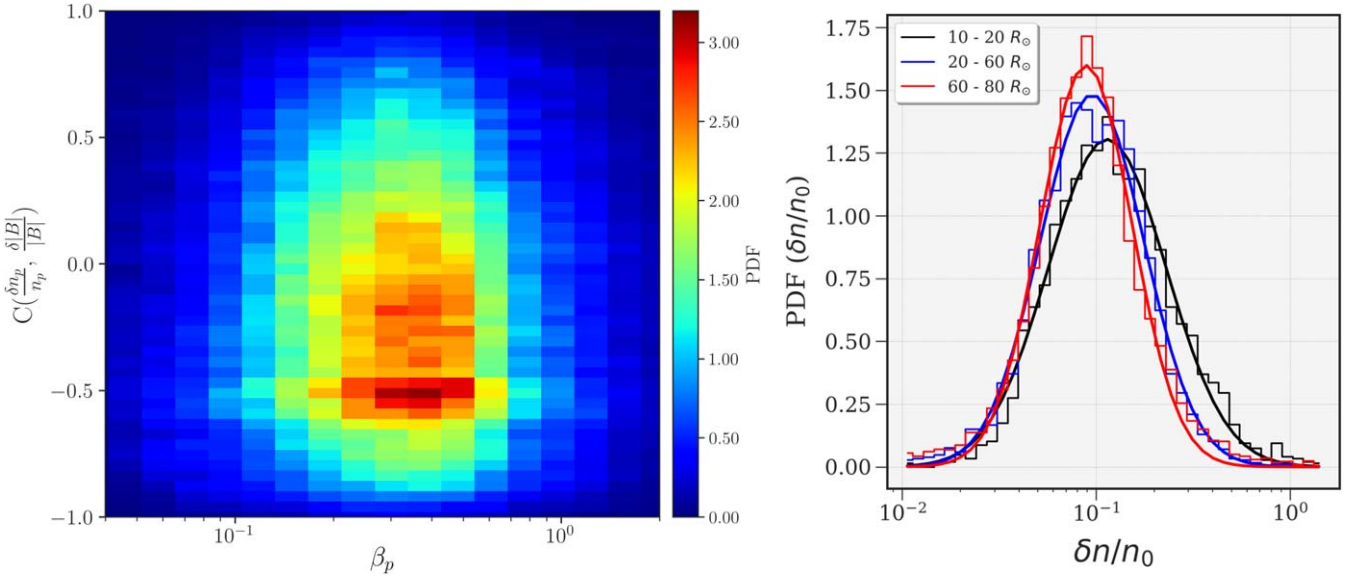

Figure 4. The left panel shows the joint distribution function of the cross correlation between the magnetic field magnitude fluctuations $\delta|B|/|B|$ and proton density fluctuations $\delta n_p/n_p$ using the present PSP data set. The right panel shows the probability density function (PDF) of the normalized density fluctuations in three different radial distance ranges using both PSP and SolO data sets. The solid curves represent the lognormal distribution fits.

where M_t is much larger than previously observed values (about 0.1) at and above 0.3 au.

2. The solar wind intervals with transonic turbulence (i.e., $M_t \sim 1$) are observed in situ by PSP measurements, and most of them are located near the Alfvén critical surface. The observation of transonic turbulence is mainly due to the fact that the amplitude of velocity fluctuations increases steadily with decreasing distance from the Sun until about 11 $R_\odot$. The decrease in sound speed with increasing radial distance is not obvious due to the local heating processes.

3. The scaling relation between the density fluctuation $\delta\rho/\rho_0$ and M_t changes from a linear scaling ($\delta\rho/\rho_0 \sim M_t$) at larger radial distances (e.g., $r > 40\,R_\odot$) gradually to a square scaling ($\delta\rho/\rho_0 \sim M_t^2$) at smaller radial distances (e.g., $10 < r < 20\,R_\odot$). The reason could be due to changes in plasma conditions near the Sun (e.g., sampling effects, low-beta regime, and high imbalance) or to changes in the nature of the compressive fluctuations.

4. Comparing transonic ($M_t \sim 1$) and subsonic ($M_t < 1$) turbulent flows when other solar wind parameters (e.g., radial distance, sampling angle, plasma beta, and cross helicity) are similar, we find that the power spectra of density fluctuations become flatter with increasing M_t values, and the spectral index of magnetic trace fluctuations does not seem to be much affected by M_t values, with the amplitude increasing with increasing M_t.

The findings are not trivial and likely indicate important physical processes related to compressible solar wind turbulence near the Sun. The SolO data set used in this paper is between ∼60 and 80 $R_\odot$, and the PSP data set is between ∼11 and 60 $R_\odot$. The SolO observations of M_t and $\delta\rho/\rho_0$ and the scaling relation between the two are consistent with the earlier mission Helios observations at similar radial distances (e.g., L. Klein et al. 1993). We note that the data sets from the two spacecraft used in this Letter do not overlap in radial distance. However, even at a given radial distance, different types of solar wind streams may be observed with different values of solar wind parameters. From a statistical point of view, the differences between PSP and SolO measurements of M_t and other parameters (i.e., M_A and β) are not severely affected by different instruments sampling different plasmas but rather statistically reflect the evolution of these plasma parameters with radial distance from the Sun.

In situ observation of heliospheric transonic turbulence $M_t \sim 1$ has not been reported before. The amplitude of the unnormalized velocity fluctuations decreases with increasing radial distance by about $r^{-1.4}$ as shown in Figure 1. The presence of transonic turbulence in the near-Sun solar wind is most likely due to the large amplitude of velocity fluctuations near the Alfvén surface (H. Wu et al. 2021; G. Zank et al. 2022; L.-L. Zhao et al. 2022b). According to remote sensing observations, within the Alfvén critical surface (about 10–15 $R_\odot$), the amplitude of velocity fluctuations will decrease as one gets closer to the Sun (S. R. Cranmer et al. 2017), which causes M_t to increase with increasing radial distance from the Sun, reach a peak value slightly above unity near the Alfvén critical surface, and then decrease with increasing radial distance. This radial evolution trend of M_t has been verified by 3D global MHD simulations (X. Fu et al. 2022; Z. Gan et al. 2023).

It may be expected that supersonic turbulence ($M_t > 1$) will generate shock-like structures. Such compressible fluctuations are expected to have a steeper power spectrum like Burgers turbulence in the inertial range, i.e., $E(k) \sim k^{-2}$, which is caused by a collection of discontinuities (e.g., S. S. Girimaji & Y. Zhou 1995; E. A. Kuznetsov 2004; T. White et al. 2019). However, this is not what we find observationally. On the contrary, our case study suggests that the observed frequency spectrum in the transonic regime ($M_t \sim 1$) departs more from f^{-2} than in the subsonic ($M_t < 1$) regime. This may be related to the low plasma beta condition. It is known that the phase velocity of the fast magnetosonic mode is close to the local Alfvén speed in the low-beta limit (i.e., $c_s \ll V_A$), while the slow magnetosonic wave is, by contrast, an ion acoustic mode with a phase velocity close to the local sound speed. The reason why the f^{-2} spectrum is not formed in the $M_t \sim 1$ interval shown in Figure 5 may be that the fluctuation speed δV may not be large enough to be superfast magnetosonic (i.e., exceed the

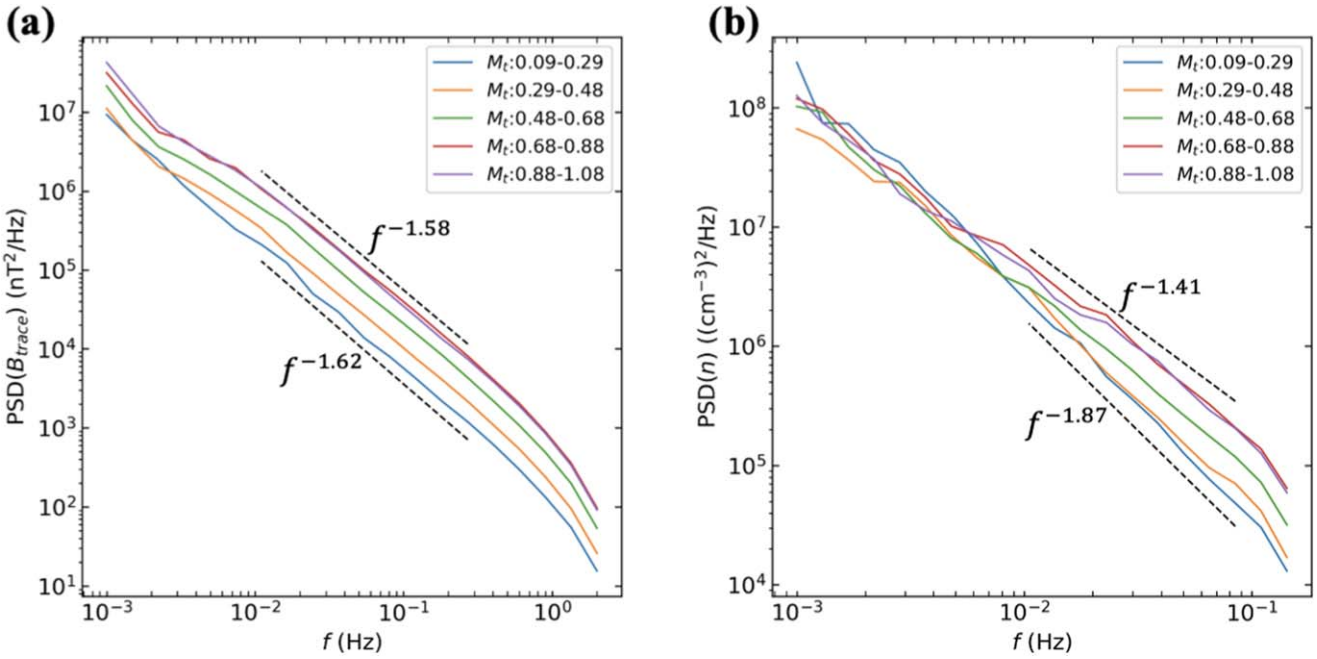

Figure 5. The wavelet power spectral density (PSD) of the total trace magnetic fluctuations (left panel) and proton density fluctuations (right panel) for different turbulent sonic Mach number M_t ranges. The black dashed lines indicate the power-law fits in the frequency range from 10^{-2} to 10^{-1} Hz.

fast wave speed) although it is close to or slightly greater than the local sound speed. This may indicate that fast magnetosonic modes rather than slow modes play a role for the transonic turbulence observed near the Sun. Linear mode decomposition (L.-L. Zhao et al. 2022b; G. Zank et al. 2023; A. Raboonik et al. 2024) will be examined elsewhere to compare the relative contribution of each MHD wave mode in transonic and subsonic turbulence, respectively. We note that the spectra shown in Figure 5 do not distinguish between sub-Alfvén and super-Alfvén bulk flows. The observed 1D reduced frequency spectra need to be converted into wavenumber spectra to explain the turbulent spectral features. A general 4D frequency-wavenumber spectrum analysis (L.-L. Zhao et al. 2024a, 2024b) needs to be performed in the near future to resolve the wavenumber spectrum of density fluctuations when the standard Taylor hypothesis is unlikely to apply, especially for $M_A \leqslant 1$ intervals.

The gradual change of scaling relation between density fluctuation and M_t is somewhat unexpected. Although the square scaling between the two is suggested by the NI turbulence theory in a homogeneous flow (e.g., G. P. Zank & W. H. Matthaeus 1993; B. J. Vasquez & J. V. Hollweg 1999), this prediction is based on the low turbulent sonic Mach number M_t regime and also uses the plasma beta as a scaling parameter. The use of NI theory to explain the observed quadratic scaling relation remains to be determined. One caveat is that the amplitude of velocity fluctuation near the Sun is calculated by assuming it is axisymmetric about the radial direction. However, we have also used the measured tangential velocity fluctuations directly when the ion VDF is in the FOV of PSP/SPAN-I, and the gradual evolution of the scaling from linear to quadratic dependence closer to the Sun shown in Figure 3 does not change, and the exponent remains close to square at 10–20 $R_\odot$. It is possible that the scaling results are biased by the sampling effects, or the properties of the compressible fluctuations near the Sun may have changed. The observed density fluctuations could be associated with slow-mode waves generated by the parametric decay of large-amplitude Alfvén waves (X. Fu et al. 2018) or zero-frequency entropy modes (G. P. Zank et al. 2024). Solar wind MHD simulations may be used in the future to better understand turbulence in this regime (Z. Gan et al. 2024, in preparation).

Acknowledgments

We acknowledge the partial support of the NSF EPSCoR RII-Track-1 Cooperative Agreement OIA-1655280, NASA awards 80NSSC20K1783 and 80NSSC23K0415, and a NASA Parker Solar Probe contract SV4-84017. A.S. is partially supported by NASA FINESST award 80NSSC24K1867. H.L. acknowledges the support by DOE OFES program and NASA HSR program. We thank the NASA Parker Solar Probe team and ESA Solar Orbiter team for the use of data.

ORCID iDs

L.-L. Zhao https://orcid.org/0000-0002-4299-0490
A. Silwal https://orcid.org/0000-0001-6286-2106
X. Zhu https://orcid.org/0000-0002-1541-6397
H. Li https://orcid.org/0000-0003-3556-6568
G. P. Zank https://orcid.org/0000-0002-4642-6192

References

Adhikari, L., Zank, G., Zhao, L.-L., et al. 2021, A&A, 656, A6
Adhikari, L., Zank, G. P., Telloni, D., et al. 2024, ApJ, 966, 52
Adhikari, L., Zank, G. P., Telloni, D., & Zhao, L.-L. 2022, ApJL, 937, L29
Adhikari, L., Zank, G. P., Zhao, L.-L., et al. 2020, ApJS, 246, 38
Bale, S., Badman, S., Bonnell, J., et al. 2019, Natur, 576, 237
Bale, S., Goetz, K., Harvey, P., et al. 2016, SSRv, 204, 49
Bandyopadhyay, R., Chasapis, A., Chhiber, R., et al. 2018, ApJ, 866, 81
Bandyopadhyay, R., Matthaeus, W., McComas, D., et al. 2022, ApJL, 926, L1
Bavassano, B., & Bruno, R. 1995, JGRA, 100, 9475
Belcher, J. W., & Davis Leverett, J. 1971, JGR, 76, 3534
Bhattacharjee, A., Ng, C., & Spangler, S. 1998, ApJ, 494, 409
Bowen, T. A., Badman, S., Hellinger, P., & Bale, S. D. 2018, ApJL, 854, L33
Bruno, R., & Carbone, V. 2013, LRSP, 10, 2

Burlaga, L., & Szabo, A. 1999, SSRv, 87, 137
Case, A. W., Kasper, J. C., Stevens, M. L., et al. 2020, ApJS, 246, 43
Chen, C. H. K., Bale, S. D., Bonnell, J. W., et al. 2020, ApJS, 246, 53
Chhiber, R., Pecora, F., Usmanov, A. V., et al. 2024, MNRAS, 533, L70
Cho, J., & Lazarian, A. 2002, PhRvL, 88, 245001
Cho, J., & Lazarian, A. 2003, MNRAS, 345, 325
Coleman, P. J., Jr. 1968, ApJ, 153, 371
Cranmer, S. R., Gibson, S. E., & Riley, P. 2017, SSRv, 212, 1345
Cuesta, M. E., Chhiber, R., Fu, X., et al. 2023, ApJL, 949, L19
Dakeyo, J.-B., Maksimovic, M., Démoulin, P., Halekas, J., & Stevens, M. L. 2022, ApJ, 940, 130
Dasso, S., Milano, L. J., Matthaeus, W. H., & Smith, C. W. 2005, ApJL, 635, L181
Del Zanna, L., Velli, M., & Londrillo, P. 2001, A&A, 367, 705
Du, S., Li, H., Fu, X., & Gan, Z. 2023, ApJ, 948, 72
Ervin, T., Bale, S. D., Badman, S. T., et al. 2024, ApJ, 972, 129
Fu, X., Li, H., Guo, F., Li, X., & Roytershteyn, V. 2018, ApJ, 855, 139
Fu, X., Li, H., Gan, Z., Du, S., & Steinberg, J. 2022, ApJ, 936, 127
Gan, Z., Fu, X., Li, H., & Du, S. 2023, AGU Fall Meeting, 2656, SH51E–2656
Girimaji, S. S., & Zhou, Y. 1995, PhLA, 202, 279
Goldreich, P., & Sridhar, S. 1995, ApJ, 438, 763
González, C., Innocenti, M. E., & Tenerani, A. 2023, JPlPh, 89, 905890208
Horbury, T., Obrien, H., Blazquez, I. C., et al. 2020, A&A, 642, A9
Howes, G. G., Bale, S. D., Klein, K. G., et al. 2012, ApJL, 753, L19
Huang, J., Kasper, J. C., Larson, D. E., et al. 2023, ApJS, 265, 47
Hunana, P., & Zank, G. P. 2010, ApJ, 718, 148
Jiao, Y., Liu, Y. D., Cheng, W., Ran, H., & Wang, R. 2024, ApJL, 975, L41
Kasper, J., Klein, K., Lichko, E., et al. 2021, PhRvL, 127, 255101
Kasper, J. C., Abiad, R., Austin, G., et al. 2016, SSRv, 204, 131
Kawazura, Y., Schekochihin, A., Barnes, M., et al. 2020, PhRvX, 10, 041050
Khotyaintsev, Y. V., Graham, D. B., Vaivads, A., et al. 2021, A&A, 656, A19
Klein, L., Bruno, R., Bavassano, B., & Rosenbauer, H. 1993, JGR, 98, 7837
Krupar, V., Szabo, A., Maksimovic, M., et al. 2020, ApJS, 246, 57
Kuznetsov, E. A. 2004, JETPL, 80, 83
Livi, R., Larson, D. E., Kasper, J. C., et al. 2022, ApJ, 938, 138
Maksimovic, M., Bale, S., Chust, T., et al. 2020, A&A, 642, A12
Malara, F., & Velli, M. 1996, PhPl, 3, 4427
Matthaeus, W. H., Klein, L. W., Ghosh, S., & Brown, M. R. 1991, JGR, 96, 5421
Moncuquet, M., Meyer-Vernet, N., Issautier, K., et al. 2020, ApJS, 246, 44
Mostafavi, P., Allen, R., Jagarlamudi, V., et al. 2024, A&A, 682, A152
Owen, C., Bruno, R., Livi, S., et al. 2020, A&A, 642, A16
Raboonik, A., Tarr, L. A., & Pontin, D. I. 2024, ApJ, 967, 80
Riley, P., Sonett, C., Tsurutani, B., et al. 1996, JGR, 101, 19987
Ruffolo, D., Thepthong, P., Pongkitiwanichakul, P., et al. 2024, ApJL, 977, L19
Salman, T. M., Nieves-Chinchilla, T., Jian, L. K., et al. 2024, ApJ, 966, 118
Shi, M., Li, H., Xiao, C., & Wang, X. 2017, ApJ, 842, 63
Smith, C. W., Vasquez, B. J., & Hamilton, K. 2006, JGRA, 111, A09111
Szabo, A., Larson, D., Whittlesey, P., et al. 2020, ApJS, 246, 47
Telloni, D., Adhikari, L., Zank, G. P., et al. 2022, ApJL, 938, L8
Telloni, D., Sorriso-Valvo, L., Woodham, L. D., et al. 2021, ApJL, 912, L21
Trotta, D., Dimmock, A., Hietala, H., et al. 2024, arXiv:2410.24007
Tu, C.-Y., & Marsch, E. 1994, JGR, 99, 21481
Tu, C. Y., & Marsch, E. 1995, SSRv, 73, 1
Usmanov, A. V., Matthaeus, W. H., Goldstein, M. L., & Chhiber, R. 2018, ApJ, 865, 25
Vasquez, B. J., & Hollweg, J. V. 1999, JGR, 104, 4681
Verdini, A., & Velli, M. 2007, ApJ, 662, 669
Verscharen, D., Chen, C. H., & Wicks, R. T. 2017, ApJ, 840, 106
Wang, J., Chhiber, R., Roy, S., et al. 2024, ApJ, 967, 150
Weygand, J. M., Matthaeus, W., Dasso, S., & Kivelson, M. 2011, JGRA, 116, A08102
White, T., Oliver, M., Mabey, P., et al. 2019, NatCo, 10, 1758
Wu, H., Tu, C., Wang, X., & Yang, L. 2021, ApJ, 922, 92
Zank, G., & Matthaeus, W. 1990, PhRvL, 64, 1243
Zank, G., Matthaeus, W., & Klein, L. 1990, GeoRL, 17, 1239
Zank, G., Zhao, L.-L., Adhikari, L., et al. 2022, ApJL, 926, L16
Zank, G., Zhao, L.-L., Adhikari, L., et al. 2023, ApJS, 268, 18
Zank, G. P., Adhikari, L., Hunana, P., et al. 2017, ApJ, 835, 147
Zank, G. P., & Matthaeus, W. H. 1992, JGR, 97, 17189
Zank, G. P., & Matthaeus, W. H. 1993, PhFlA, 5, 257
Zank, G. P., Zhao, L.-L., Adhikari, L., et al. 2024, ApJ, 966, 75
Zhao, L. L., Adhikari, L., Zank, G. P., Hu, Q., & Feng, X. S. 2017, ApJ, 849, 88
Zhao, L.-L., Zank, G., Adhikari, L., & Nakanotani, M. 2022a, ApJL, 924, L5
Zhao, L.-L., Zank, G., He, J., et al. 2021a, A&A, 656, A3
Zhao, L.-L., Zank, G., Hu, Q., et al. 2021b, A&A, 650, A12
Zhao, L.-L., Zank, G., & Li, H. 2024a, ApJL, 962, L14
Zhao, L.-L., Zank, G., Opher, M., et al. 2024b, ApJ, 973, 26
Zhao, L.-L., Zank, G., Telloni, D., et al. 2022b, ApJL, 928, L15
Zhao, L. L., Zank, G. P., Adhikari, L., et al. 2022, ApJL, 934, L36